Reply for the referee comment#1

Summary: This study examines the deposition of soluble iron from dust aerosols using the Community Atmosphere Model version 6 (CAM6-chem). CAM6-chem has been developed here to include desert dust mineralogy and to incorporate proton- and oxalate-promoted dissolution schemes for the iron-containing dust aerosols. The main focus of this work is on the factors influencing the deposition of soluble iron from dust in the Northwest Pacific during the spring seasons from 2001 to 2017, with evaluation against observational datasets from the North Pacific. The authors report a decrease in the deposition of soluble iron from East Asia to the Northwest Pacific during the studied period, which is attributed to reduced dust emissions. However, they also observe an increase in dust iron solubility, primarily linked to the atmospheric processing of coarse dust aerosols. Sensitivity simulations indicate that rising anthropogenic NOx emissions, rather than a reduction in SO2, are the primary factor influencing dust aerosol acidity in the model, leading overall to an increase in iron solubility despite the decrease in iron from dust. The manuscript is well-written; however, some issues concerning the methodology and the presentation of results should be addressed before final publication. This will help readers better understand the assumptions considered in this work along with the uncertainties surrounding the main conclusions derived from model simulations.

Summary Response: We sincerely appreciate the detailed feedback, which has significantly contributed to improving our manuscript. Below, we provide responses to each comment and describe the corresponding revisions.

General comment#1: The authors used the global model CAM6-chem to simulate the soluble iron deposition over the Northwest Pacific. Given that a number of global modelling studies provide global budget calculations of the atmospheric iron cycle (i.e., burdens, wet and dry deposition rates, iron solubilisation rates, etc.), both for total and soluble iron or per mode (fine and coarse) iron-containing aerosols, the authors should provide their global estimations along with those for the study area. I also propose to present the budget calculations in a separate table and present other modelling estimates for comparison.

Response for comment#1: Thank you for your insightful comment. We have added global and Northwest Pacific (NWP) atmospheric iron cycle budget in Table 2. This table includes burdens, wet and dry deposition rates, and iron solubilization rates for both fine and coarse dust total/soluble iron aerosols calculated from 2017 all year modelling. Additionally, we have compared our model results with the Mechanism of Intermediate complexity for Modelling Iron (MIMI) from Hamilton et al. (2019) of which the period is 2007-2011, EC-Earth model from Myriokefalitakis et al. (2022) of which the period is 2000-2014, and the ensemble modeling study of Myriokefalitakis et al. (2018) of which the period across 2007-2014. The comparison results have been shown in Table 3. We discuss the atmospheric iron cycle in line 279.

Line 279:

"3.2 Spatial and temporal characteristics of dust iron deposition

3.2.1 Atmospheric dust iron budget

…

The global annual atmospheric dust total and soluble iron budget have been presented in Table 2. The simulated global burdens of dust total and soluble iron were 1331 Gg and 15.4 Gg respectively. The simulated global dust total and soluble iron deposition were 109 and 1.3 Tg/yr aligning well with values reported by the MIMI (Table 3). Due to higher dust emissions, our simulated dust iron deposition and burdens are nearly double those of the EC-Earth and Ensemble models (Myriokefalitakis et al., 2018). For solubilization rates, the EC-Earth model reported 315 Gg/yr and 170 Gg/yr for proton-promoted and oxalate-promoted dissolution but our results indicated 129 Gg/yr and 200 Gg/yr. The lower solubilization rate of proton-promoted and higher solubilization rate of oxalate-promoted in our study could be attributed to the lower simulated coarse aerosol mode acidity and higher scaled oxalate levels than EC-Earth respectively. And the difference in simulation period and iron dissolution mechanisms would also induce discrepancy. For the Northwest Pacific, simulated dust total and soluble iron burdens were 7.4 Gg and 0.11 Gg aligning closely with Ensemble model results. Dust total and soluble iron deposition rates in this region were 589 Gg/yr and 10.1 Gg/yr consistent with both MIMI and Ensemble model estimates. But EC-Earth reported higher NWP deposition rates than our model due to differences in regional dust simulation."

Table 2. Global annual atmospheric dust total/soluble iron budget in 2017.

	Burden (Gg)		**Dry deposition (Tg/yr and Gg/yr)**		**Wet deposition (Tg/yr and Gg/yr)**		**Solu. Rate (Gg/yr)**	
	Fe_tot	Fe_sol	Fe_tot	Fe_sol	Fe_tot	Fe_sol	Fe_ps	Fe_os
Global	1331	15.4	42.7	445	66.5	874	129	200
coarse, fine	1301, 30	13.3, 2.1	42.2, 0.5	421, 24	65.4, 1.1	789, 85	78, 51	196, 4
NWP	7.4	0.11	0.05	1.2	0.54	8.9	1.3	1.73
coarse, fine	7.1, 0.3	0.09, 0.02	0.05, 0.001	1.1, 0.1	0.53, 0.01	7.8, 1.1	1.1, 0.2	1.68, 0.05

Table 3. Comparison of global annual atmospheric dust total/soluble iron budget from different studies.

		This study		**MIMI[1]**		**EC-Earth[1]**		**Ensemble[1]**	
		Fe_tot	**Fe_sol**	**Fe_tot**	**Fe_sol**	**Fe_tot**	**Fe_sol**	**Fe_tot**	**Fe_sol**
Global	**Burden (Gg)**	1331	15.4	/	/	/	6	563	10
	Deposition (Tg/yr)	109	1.3	127	1.6	59	0.6	68	0.6
NWP	**Burden (Gg)**	7.4	0.11	/	/	/	/	5.7	0.18
	Deposition (Gg/yr)	589	10.1	472	10.4	2147	33	369	7.7

1. The simulation periods are as follows: 2007-2011 for MIMI, 2000-2014 for EC-Earth, and 2007-2014 for the Ensemble.

Reference

Hamilton, D. S., Scanza, R. A., Feng, Y., Guinness, J., Kok, J. F., Li, L., Liu, X., Rathod, S. D., Wan, J. S., Wu, M., and Mahowald, N. M.: Improved methodologies for Earth system modelling of atmospheric soluble iron and observation comparisons using the Mechanism of Intermediate complexity for Modelling Iron (MIMI v1.0), Geosci. Model Dev., 12, 3835-3862, 10.5194/gmd-12-3835-2019, 2019.

Myriokefalitakis, S., Bergas-Massó, E., Gonçalves-Ageitos, M., Pérez García-Pando, C., van Noije,

T., Le Sager, P., Ito, A., Athanasopoulou, E., Nenes, A., Kanakidou, M., Krol, M. C., and Gerasopoulos, E.: Multiphase processes in the EC-Earth model and their relevance to the atmospheric oxalate, sulfate, and iron cycles, Geosci. Model Dev., 15, 3079-3120, 10.5194/gmd-15-3079-2022, 2022.

Myriokefalitakis, S., Ito, A., Kanakidou, M., Nenes, A., Krol, M. C., Mahowald, N. M., Scanza, R. A., Hamilton, D. S., Johnson, M. S., Meskhidze, N., Kok, J. F., Guieu, C., Baker, A. R., Jickells, T. D., Sarin, M. M., Bikkina, S., Shelley, R., Bowie, A., Perron, M. M. G., and Duce, R. A.: Reviews and syntheses: the GESAMP atmospheric iron deposition model intercomparison study, Biogeosciences, 15, 6659-6684, 10.5194/bg-15-6659-2018, 2018.

General comment#2: In Sect. 2, the calculation of oxalate concentrations in the model used for the ligand-promoted dissolution is not clearly explained. The authors employed the formula from Hamilton et al. (2019) to estimate atmospheric oxalate levels based on the modeled secondary organic carbon concentrations. However, Hamilton et al. (2019) established a maximum aqueous concentration threshold of 15 μmol L^{-1}, derived from the estimations of Scanza et al. (2018). What threshold is applied here? Do the authors calculate with their model version similar secondary organic carbon concentrations as reported by Scanza et al. (2018) and Hamilton et al. (2019)? If it differs, what threshold was used? Additionally, how might this assumption affect the simulated oxalate concentrations?

Response: Thank you for your insightful comment. Below, we address the key points raised:

(1) Threshold Consistency

We employed the same maximum aqueous oxalate concentration threshold of 15 μmol L^{-1}, consistent with Hamilton et al. (2019) and Scanza et al. (2018).

(2) Comparison of Secondary Organic Aerosols (SOA) Models

Hamilton et al. (2019) employed the CAM versions 5 and 6 (CESM-CAM5–6; Neale et al., 2010). In our study, the version CAM6-Chem coupled with MOSAIC was used.

In CAM5 and CMA6, SOA is simulated through the pre-calculated, lumped SOA gas-phase species undergoing reversible condensation and evaporation into aerosols. This gas-phase SOA precursor (SOAG) is derived from fixed mass yields for five categories of volatile organic compounds (VOCs) with yields increased by 50% after tuning for aerosol indirect effects (Neale et al., 2010; Liu et al., 2012).

In CAM6-Chem, SOA formation follows a Volatility Basis Set (VBS) approach with explicit VOCs and chemistry (Emmons et al., 2020; Tilmes et al., 2019). It incorporates wall-corrected SOA yields, photolytic removal of SOA, and more efficient removal by dry and wet deposition. In addition, the CAM6-Chem model applied in our study also simulates the heterogeneous uptake of isoprene epoxydiols (IEPOX) onto sulfate aerosols and production of IEPOX-SOA (Jo et al., 2019; 2021).

The simulated SOA burden was 1.15 Tg/yr in CAM5 (2001-2006; Liu et al., 2012), 1.07 Tg/yr in CAM6 (1995-2010; Tilmes et al., 2019) and 1.02 Tg/yr in CAM6-Chem (2013; Jo et al., 2023). In terms of SOA mechanism used by our study, the SOA burden was 1.42 Tg/yr during 2001-2017 which is little higher but comparable with the 1.15 Tg/yr in CAM5 as used by Hamilton et al. (2019).

Furthermore, the spatial distribution has been shown in Figure S3 and it is comparable with the results (Fig. 3a) from CAM5 (Liu et al., 2012). Specifically, the maximum secondary organic carbon concentrations calculated in our model during 2001-2017 is close to the number (1.41 vs 1.41 mol/mol) used in Hamilton et al. (2019). Based on this consistency, we chose not to alter the parameters in the formula from Hamilton et al. (2019). As a result, the scaled oxalate concentrations align well with the observational data especially in East Asia as shown in Figure S4.

(3) Impact on Oxalate Estimation and future work

Differences in SOA concentrations in our study could lead to overestimation of oxalate concentrations and the subsequent oxalate-promoted soluble iron contribution. However, Hamilton et al. (2019) did not analyze the relative contributions of proton-promoted and oxalate-promoted processes. This makes it challenging to determine whether oxalate-promoted contributions are consistently over- or underestimated in our study. We acknowledge this limitation and emphasize the need for direct oxalate concentration calculations in future work to improve simulation accuracy.

We have made a further discussion in line 80 and line 179.

Line 80:

"In CAM6-Chem, SOA formation follows a Volatility Basis Set (VBS) approach with explicit VOCs and chemistry (Emmons et al., 2020; Tilmes et al., 2019). It incorporates wall-corrected SOA yields, photolytic removal of SOA, and more efficient removal by dry and wet deposition. What's more, the heterogeneous uptake of isoprene epoxydiols (IEPOX) onto sulfate aerosols and their subsequent production are explicitly simulated through coupling with MOSAIC (Jo et al., 2019; 2021)."

Line 179:

"The threshold of oxalate concentration is 15 μmol L^{-1} keeping consistent with Hamilton et al. (2019) and Scanza et al. (2018). Because the SOA burden simulated in our model version (Figure S3) is comparable with the previous version (Fig. 5a; Liu et al., 2012). The maximum SOA concentration was similar to the study of Hamilton et al. (2019). For the oxalate evaluation, … our model accurately captures the quantitative characteristics of oxalate especially in East Asia (Figure S4)."

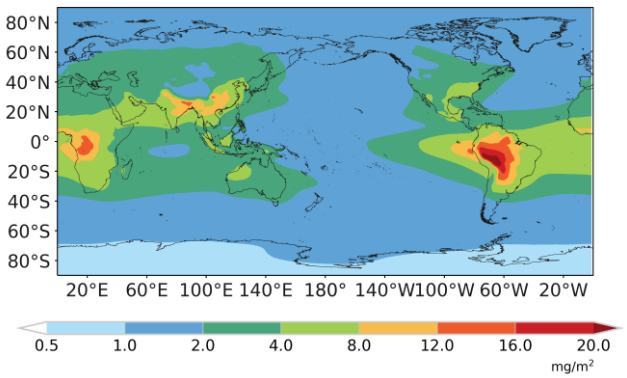

Figure S3. Spatial distribution of Secondary Organic Aerosols (SOA) burden from 2001 to 2017 with simulation data from Liu et al. (2023).

Reference

Emmons, L. K., Schwantes, R. H., Orlando, J. J., Tyndall, G., Kinnison, D., Lamarque, J.-F., Marsh, D., Mills, M. J., Tilmes, S., Bardeen, C., Buchholz, R. R., Conley, A., Gettelman, A., Garcia, R., Simpson, I., Blake, D. R., Meinardi, S., and Pétron, G.: The Chemistry Mechanism in the Community Earth System Model Version 2 (CESM2), Journal of Advances in Modeling Earth Systems, 12, e2019MS001882, https://doi.org/10.1029/2019MS001882, 2020.

Jo, D. S., Tilmes, S., Emmons, L. K., Wang, S., and Vitt, F.: A new simplified parameterization of secondary organic aerosol in the Community Earth System Model Version 2 (CESM2; CAM6.3), Geosci. Model Dev., 16, 3893-3906, 10.5194/gmd-16-3893-2023, 2023.

Jo, D. S., Hodzic, A., Emmons, L. K., Marais, E. A., Peng, Z., Nault, B. A., Hu, W., Campuzano-Jost, P., and Jimenez, J. L.: A simplified parameterization of isoprene-epoxydiol-derived secondary organic aerosol (IEPOX-SOA) for global chemistry and climate models: a case study with GEOS-Chem v11-02-rc, Geosci. Model Dev., 12, 2983-3000, 10.5194/gmd-12-2983-2019, 2019.

Liu, X., Easter, R. C., Ghan, S. J., Zaveri, R., Rasch, P., Shi, X., Lamarque, J. F., Gettelman, A., Morrison, H., Vitt, F., Conley, A., Park, S., Neale, R., Hannay, C., Ekman, A. M. L., Hess, P., Mahowald, N., Collins, W., Iacono, M. J., Bretherton, C. S., Flanner, M. G., and Mitchell, D.: Toward a minimal representation of aerosols in climate models: description and evaluation in the Community Atmosphere Model CAM5, Geosci. Model Dev., 5, 709-739, 10.5194/gmd-5-709-2012, 2012.

Liu, Y., Dong, X., Emmons, L. K., Jo, D. S., Liu, Y., Shrivastava, M., Yue, M., Liang, Y., Song, Z., He, X., and Wang, M.: Exploring the Factors Controlling the Long-Term Trend (1988–2019) of Surface Organic Aerosols in the Continental United States by Simulations, Journal of Geophysical Research: Atmospheres, 128, e2022JD037935, https://doi.org/10.1029/2022JD037935, 2023.

Tilmes, S., Hodzic, A., Emmons, L. K., Mills, M. J., Gettelman, A., Kinnison, D. E., Park, M., Lamarque, J.-F., Vitt, F., Shrivastava, M., Campuzano-Jost, P., Jimenez, J. L., and Liu, X.: Climate Forcing and Trends of Organic Aerosols in the Community Earth System Model (CESM2), Journal of Advances in Modeling Earth Systems, 11, 4323-4351, https://doi.org/10.1029/2019MS001827, 2019.

Neale, R., Gettelman, A., Park, S., Chen, C.-C., Lauritzen, P. H., Williamson, D., Conley, A. J., Kinnison, D. E., Marsh, D., Smith, A. K., Vitt, F. M., Rolando R. García, Lamarque, J.-F., Mills, M. J., Tilmes, S., Morrison, H., Cameron-Smith, P., Collins, W., Iacono, M. J., … Taylor, M. A. (2012). Description of the NCAR Community Atmosphere Model (CAM 5.0). https://doi.org/10.5065/wgtk-4g06 (Original work published 2012)

General comment#3: The authors note that the model accurately captures oxalate observations. However, in Sect. 3.3.3, only the simulated surface oxalate concentration patterns over EA are presented, with no evaluation of the modeled OXL concentrations against observations. As far as I understand, the authors only compare spatial patterns from other modeling studies. I suggest that the authors present an evaluation of their model using observations (both globally and with a special focus on the EA region), as done in the other studies referenced in the manuscript.

Response: Thanks for the comment. We collected global oxalate observations in rain/cloud water to provide a more detailed comparison. The references have been listed in supplementary. Figures S4 in the supplementary material show the spatial distribution of observation locations and the evaluation of the simulation. We have expanded the oxalate comparison in line 182 as follows:

Line 181: "For the oxalate evaluation, we have collected global oxalate observations in rain/cloud water to evaluate our model results. The locations and months are consistent between observations and the model. Comparisons with observed oxalate levels indicate that our model accurately captures the quantitative characteristics of oxalate especially in East Asia (Figure S4)."

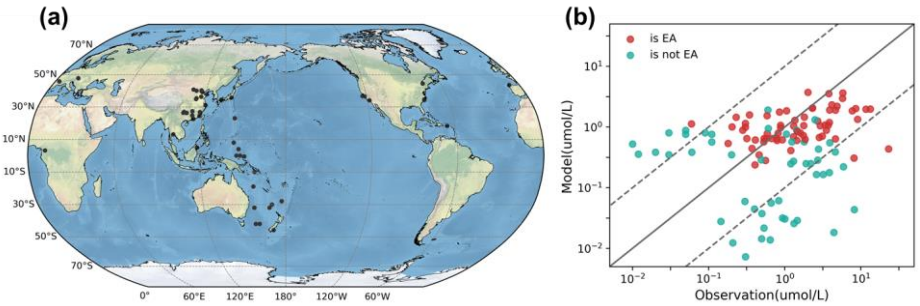

Figure S4. (a) Sample locations of the observed oxalate in rain/cloud water (Sempéré and Kawamura, 1996; Willey et al., 2000; Brooks Avery et al., 2001; Kawamura et al., 2001; Hegg et al., 2002; Kieber et al., 2002; Löflund et al., 2002; Peña et al., 2002; Kim et al., 2003; Sigha-Nkamdjou et al., 2003; Crahan et al., 2004; Hu et al., 2005; Brooks Avery et al., 2006; Xu et al., 2009; Huang et al., 2010; Huo et al., 2010; Sumari et al., 2010; Gioda et al., 2011; Wang et al., 2011; Zhang et al., 2011; Khuntong, 2012; Zhu et al., 2016; Du et al., 2017; Zhao et al., 2019; Zhang et al., 2021; González et al., 2022; Lee et al., 2022; Xie et al., 2022; Sun et al., 2024). (b) The comparison between estimated oxalate concentration in cloud water and observations.

General comment#4: It is unclear how ligand-promoted dissolution is limited under cloud conditions in the model. I would expect a more detailed discussion of the cloud parameters that influence oxalate production, such as liquid water content (LWC) and cloud cover, as well as how these factors are incorporated into the process of oxalate-promoted iron dissolution.

Response: Thanks for your insightful comment. Previous studies demonstrated that oxalate ligand complexation reaction proceeds within cloud environments. And the oxalate-promoted processing rates are measured in water used in our study from Paris et al. (2011). Hence, the oxalate-promoted processing only occurs in cloud environment set by our model as well as the study of Hamilton et al. (2019). Specifically, the cloud environment represented the cloud fraction is higher than 1E-5

and cloud liquid water content (LWC) is higher than 1E-8 (L/L(cloud)) in the model. The possibility of oxalate-promoted processing would increase if the cloud fraction and LWC increase. In the study area, we used the cloud fraction as an indicator to show the trend of cloud (Fig. 9e). Apart from the increased cloud faction, the temporal LWC was also increased and we added it as Figure S16. We have expanded the discussion in line 470 and line 493.

Line 470: "Specifically, the cloud environment represents the cloud fraction is higher than 1E-5 and cloud liquid water content (LWC) is higher than 1E-8 (L/L(cloud)) in the model. The possibility of oxalate-promoted processing would increase if the cloud fraction and LWC increase. Hence, we focus our analysis on two factors including oxalate concentration and cloud fraction which is a proxy of cloud environment in this section."

Line 494: "Similarly, the temporal LWC was also increased as shown in Figure S16. The increased cloud fractions and LWC would provide more possibility for oxalate-promoted processing as it only occurs in the cloud borne phase, thereby enhancing oxalate-promoted soluble iron production."

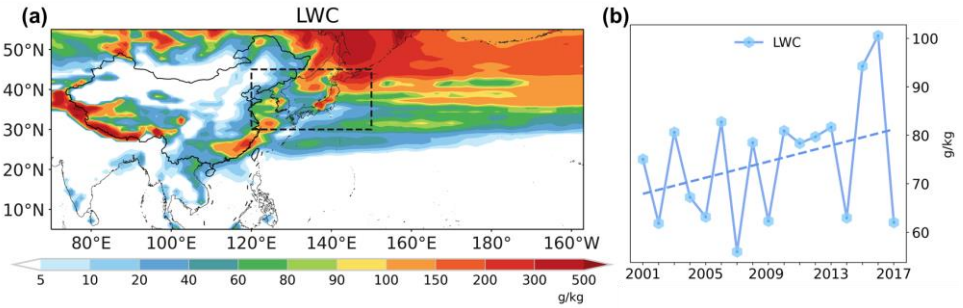

Figure S16. (a) Spatial distributions of surface cloud liquid water content averaged of 2001-2017 springs. (b) Temporal variations of surface cloud liquid water content over high production rate area (30-45N, 120-150E) averaged of 2001-2017 springs.

Reference

Hamilton, D. S., Scanza, R. A., Feng, Y., Guinness, J., Kok, J. F., Li, L., Liu, X., Rathod, S. D., Wan, J. S., Wu, M., and Mahowald, N. M.: Improved methodologies for Earth system modelling of atmospheric soluble iron and observation comparisons using the Mechanism of Intermediate complexity for Modelling Iron (MIMI v1.0), Geosci. Model Dev., 12, 3835-3862, 10.5194/gmd-12-3835-2019, 2019.

Paris, R., Desboeufs, K. V., and Journet, E.: Variability of dust iron solubility in atmospheric waters: Investigation of the role of oxalate organic complexation, Atmospheric Environment, 45, 6510-6517, https://doi.org/10.1016/j.atmosenv.2011.08.068, 2011.

General comment#5: How much are the globally averaged dust emissions in the model? How is the emitted iron distributed between the fine (Aitken and accumulation) and coarse modes at dust emissions? What is the simulated global mean percentage of iron in dust? Additionally, what is the initial Fe solubility in dust? It would be beneficial for the reader to present some values used in the model, preferably in a separate table, instead of simply referring to the original publications.

Response: Thanks for your insightful comment. We have added the Table S3 which contained the global emissions of dust, dust total iron, dust soluble iron in fine and coarse mode, as well as the global mean iron content in dust and dust iron solubility. A discussion has been added in Section 3.2 in combination with General Comment #1.

Line 272:

"3.2 Spatial and temporal characteristics of dust iron deposition

3.2.1 Atmospheric dust iron budget

The global mean emissions of dust, dust total iron, and dust soluble iron were 2707 Tg/yr, 109 Tg/yr, and 0.98 Tg/yr, respectively, based on our 2017 model simulation (Table S3). These values are comparable to those reported by the Mechanism of Intermediate complexity for Modelling Iron (MIMI) model (Hamilton et al., 2019) (3200 Tg/yr and 130 Tg/yr for dust and dust total iron emissions) but are approximately twice as high as the results from EC-Earth model (Myriokefalitakis et al., 2022) (1265 Tg/yr and 59.3 Tg/yr). The simulated global mean iron content in dust is 4.0% which aligns well with MIMI (4.1%) and EC-Earth (4.7%). The initial iron solubility is 0.91% and higher than the 0.1% set by EC-Earth."

Table S3. Global emissions of dust, dust total/soluble iron in 2017.

	Dust	Total iron	Soluble iron	Iron content	Iron solubility
Emissions (Tg/yr)	2707	109	0.98	4.0%	0.91%
coarse mode	2677	107	0.93	3.9%	0.88%
fine mode	30	2	0.05	5.3%	3.4%

General comment#6: The authors indicate that oxalate-promoted processing accounts for 25% of total soluble iron deposition from dust, approximately double that of proton-promoted processing. This finding is noteworthy, as it contradicts other studies suggesting an alternative perspective. For example, Ito and Shi (2016) reported that the proton-promoted dissolution scheme contributed the majority of soluble iron deposition to the ocean, while Myriokefalitakis et al. (2022) found that proton-promoted dissolution is the primary process for dust aerosols, whereas ligand-promoted dissolution is considered more significant for combustion aerosols (which are not addressed in this study). Could this outcome of the model indicate an underestimation of aerosol acidity or an overestimation of oxalate concentrations within the model? Is this result only attributable to coarse-mode dust? Could you please provide further elaboration on this finding?

Response: Thanks for your insightful comment. Below, we address the key aspects of the oxalate-promoted versus proton-promoted soluble iron contributions:

(1) Relative Contributions from Different Processes

The relative contributions of emissions, proton-promoted and oxalate-promoted to Northwest Pacific dust soluble iron deposition in coarse and fine modes are presented in Figure S8. Our findings highlight the dominant role of oxalate-promoted processing, particularly in the coarse mode as you mentioned. For the fine mode, proton-promoted processing accounts for approximately 39% of the soluble iron deposition which is about six times higher than oxalate-promoted processing. We have added Figure S8 and expanded the discussion in line 331 to further clarify these contributions.

(2) Consistency with Previous Studies

Globally and over East Asia, our study shows oxalate-promoted processing dominates atmospheric soluble iron deposition. This result aligns with the findings of Scanza et al. (2018), which demonstrated the significant role of oxalate-promoted processing using the CAM4 model. Additionally, observational data from the Qingdao station (Shi et al., 2022) further corroborate the critical role of oxalate in soluble iron deposition.

(3) Differences Between Models

Compared to the observations, the estimated oxalate in our model showed no significant over- or underestimation especially over the East Asia (Figure S8). Based on Figure 6g in Myriokefalitakis et al. (2022) and figure S3 in Ito (2015), oxalate concentrations appear to be underestimated. This suggests that the role of oxalate-promoted dissolution might also be underestimated in their model. In terms of proton-promoted processing, the simulated mainland coarse-mode aerosol acidity in our model (Figure S2) is obviously lower than that in EC-Earth (Fig. S3e; Myriokefalitakis et al., 2022) and IMPACT model (Fig. S2b; Ito and Xu, 2014). This could explain the reduced contribution of proton-promoted dissolution for dust soluble iron in our results compared to EC-Earth and IMAPACT. But The lack of sufficient observations makes it challenging to provide a detailed comparison for the model performance with respect to coarse mode aerosols. What's more, the acidity of fine aerosols simulated in our model have been validated by comparing with observationally estimated pH (Figure S2) showed no significant over- or underestimation.

(4) Model Limitations and Uncertainties

The higher contribution of oxalate-promoted dissolution in our study might be partially attributed to differences in the parameterization of oxalate concentrations and aerosol acidity between models. As discussed in General Comment #2, the limitations of our oxalate estimation method could also introduce uncertainties. To refine the relative contributions of ligand- and proton-promoted dissolution, we emphasize the importance of further observational constraints on oxalate concentrations, aerosol acidity, and their interactions in soluble iron production. Future studies should focus on improving these aspects to enhance model accuracy. We have made a further discussion in line 318.

Line 318: "Throughout the springs of 2001-2017, the NWP received an average of 4.9 Gg/season of soluble iron deposition from EA (Figure 5). The relative contributions of emissions, proton-promoted and oxalate-promoted to Northwest Pacific dust soluble iron deposition in coarse and fine modes are presented in Figure S8. Atmospheric processing played a significant role (~40%) in dust soluble iron deposition of which the oxalate ligand-promoted processing emerged as a dominant contributor (25%). The contribution of the oxalate-promoted processing was about twice that of

proton-promoted processing. And this result is consistent with previous modelling (Johnson and Meskhidze, 2013; Scanza et al., 2018) and observation research (Shi et al., 2022). Differently, Ito and Shi (2016) and Myriokefalitakis et al. (2022) found that proton-promoted dissolution is the primary process. The higher contribution of oxalate-promoted dissolution in our study might be partially attributed to differences in the parameterization of oxalate concentrations and aerosol acidity between models. As the oxalate concentrations appear to be underestimated in their model and the simulated mainland coarse-mode aerosol acidity in our model (Figure S2) is obviously lower than those. Future studies should focus on improving these aspects to refine the relative contributions of atmospheric processing."

Line 331: "And The dominant role of oxalate-promoted processing was mainly determined by the coarse mode (Figure S8). For the fine mode, proton-promoted processing accounts for approximately 39% of the soluble iron deposition which is about six times higher than oxalate-promoted processing."

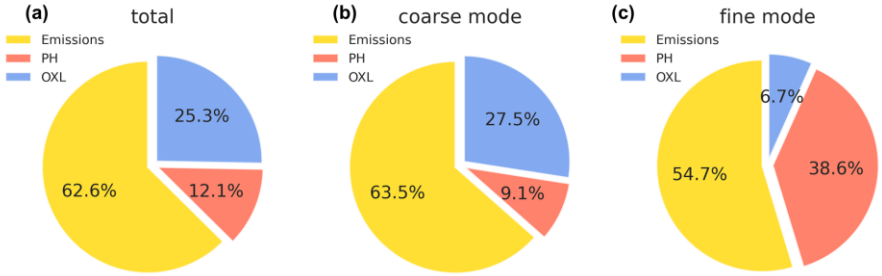

Figure S8. Relative contributions of emissions, oxalate-promoted, and proton-promoted processing to the Northwest Pacific dust soluble iron deposition averaged of 2001-2017 springs in total (a), coarse mode (b), and fine mode (c).

Reference

Ito, A.: Atmospheric Processing of Combustion Aerosols as a Source of Bioavailable Iron, Environmental Science & Technology Letters, 2, 70-75, 10.1021/acs.estlett.5b00007, 2015.

Ito, A. and Xu, L.: Response of acid mobilization of iron-containing mineral dust to improvement of air quality projected in the future, Atmos. Chem. Phys., 14, 3441-3459, 10.5194/acp-14-3441-2014, 2014.

Myriokefalitakis, S., Bergas-Massó, E., Gonçalves-Ageitos, M., Pérez García-Pando, C., van Noije, T., Le Sager, P., Ito, A., Athanasopoulou, E., Nenes, A., Kanakidou, M., Krol, M. C., and Gerasopoulos, E.: Multiphase processes in the EC-Earth model and their relevance to the atmospheric oxalate, sulfate, and iron cycles, Geosci. Model Dev., 15, 3079-3120, 10.5194/gmd-15-3079-2022, 2022.

Scanza, R. A., Hamilton, D. S., Perez Garcia-Pando, C., Buck, C., Baker, A., and Mahowald, N. M.: Atmospheric processing of iron in mineral and combustion aerosols: development of an intermediate-complexity mechanism suitable for Earth system models, Atmos. Chem. Phys., 18, 14175-14196, 10.5194/acp-18-14175-2018, 2018.

Shi, J., Guan, Y., Gao, H., Yao, X., Wang, R., and Zhang, D.: Aerosol Iron Solubility Specification in the Global Marine Atmosphere with Machine Learning, Environmental Science & Technology, 56, 16453-16461, 10.1021/acs.est.2c05266, 2022.

General comment#7: In Fig. S2b, a weak correlation is observed in the evaluation of pH. Could you please provide relevant statistics and discuss potential reasons for the misrepresentation of atmospheric acidity in the model? It is expected that fine particles are relatively more acidic due to nss-sulfate and other acidic compounds contributions, while the coarse mode, which includes sea salt and dust, is much less acidic. Can you provide figures of the calculated pH values for each aerosol mode of the model?

Response: Thank you for your insightful comment. The evaluation of fine mode pH is based on observationally estimated ground-level fine-aerosol pH and annually averaged simulated values at consistent locations. The correlation coefficient and normalized mean bias (NMB) are 0.4 and 27% respectively. Regarding the potential reasons for the misrepresentation of atmospheric acidity in the model: We directly utilize the annually averaged simulated aerosol pH to compare with observations from different months. Hence, the seasonal variations may introduce discrepancies of approximately ±1 in the pH values. What's more, the dynamic changes of precursor gas emissions, environmental factors such as relative humidity could also induced discrepancy of modelled aerosol acidity.
We also have added figures of the calculated pH values for the accumulation mode and coarse mode aerosols as Figure S2 These figures clearly illustrate that fine particles are relatively more acidic while coarse-mode particles are significantly less acidic influenced by sea salt and dust components.

We have made a further discussion in line 158.

Line 158: "The simulated aerosol pH in accumulation and coarse mode have been shown in Figure S2. The fine particles are relatively more acidic while coarse-mode particles are significantly less acidic influenced by sea salt and dust components. Through the annually averaged comparison of accumulation mode aerosols' pH with observations collected by Pye et al. (2020), our model successfully captured the global characteristics of fine aerosol pH. The correlation coefficient and normalized mean bias (NMB) are 0.4 and 27% respectively. The discrepancy could be attributed by the seasonal variations and the dynamics of precursor gas emissions, environmental factors such as relative humidity."

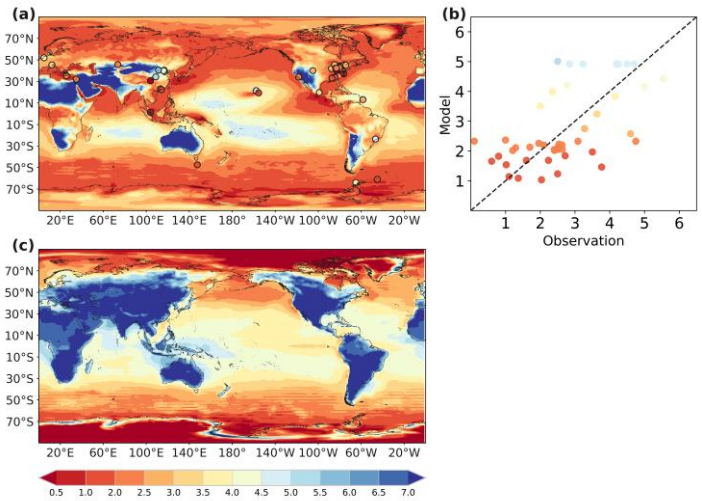

Figure S2. (a) Spatial distribution of aerosol pH in accumulation mode in 2013 and observationally estimated ground-level fine-aerosol pH (dots) from Pye et al. (2020). (b) The linear relationship between aerosol pH simulation and observationally estimated ground-level fine-aerosol pH. (c) Spatial distribution of aerosol pH in coarse mode in 2013.

General comment#8: As a final comment, while the paper focuses on the deposition of soluble iron from dust aerosols, the omission of pyrogenic iron complicates a fair comparison with atmospheric observations. Numerous recent studies underscore the importance of pyrogenic iron from downwind source regions similar to the one examined here. It is unclear why the authors did not also include pyrogenic iron emissions in their analysis, especially since other versions of the model did. Consequently, when evaluating a model against observational data, the authors should preferably select cases where iron-containing dust aerosols predominantly influence the measured concentrations (e.g., by utilizing back trajectories). However, it is not clear whether this approach was implemented in the current study. Could you please provide some clarification on this?

Response: Thank you for your insightful comment. The primary goal of this study is to evaluate the trends in dust-derived soluble iron deposition which is most pronounced during the spring seasons when East Asian dust emissions significantly impact the Northwest Pacific. Pyrogenic iron emission shall not be a key factor to the analysis of long-term trend of natural dust iron, especially our analysis was made for spring only. For instance, the pyrogenic soluble iron deposition to the Northwest Pacific account for 36% of total soluble iron deposition from 1980 spring to 2014 spring (Hamilton et al., 2020), indicating dust shall be the dominant sources during spring. What's more, the uncertainties in current pyrogenic iron emission inventories (Ito et al., 2023; Rathod et al., 2020; Liu et al., 2024) make it challenging to incorporate this source accurately. Therefore, we did not include pyrogenic iron in our analysis as our focus remains on dust as the dominant contributor to soluble iron during the spring season. But the anthropogenic soluble iron deposition to the Northwest Pacific presented an obvious trend (increased ~1Gg/season) from 2001 spring to 2014 spring from the study of Hamilton et al. (2020). The increased trend could opposite the decreased dust soluble iron deposition to some extent. We have expanded the discussion in line 545.

The observations of iron used here is the total iron which include dust and pyrogenic iron. Our model only captures the 0-10% iron solubility (Figure S7). This might be due to the lack of

pyrogenic iron which has been suggested to contribute to higher iron solubility (Ito et al., 2019). To address the potential influence of mixed iron sources, we performed preliminary back-trajectory analyses for selected cases which presented three dust events during springs (Buck et al., 2013; Chen 2004). But the back-trajectory analysis cannot fully distinguish between dust and pyrogenic iron contributions, especially as air masses pass over regions like the North China Plain which may introduce anthropogenic influences in springs (showed below). We have clarified the limitation of observations and expanded the discussion in line 267.

Line 545: "It is crucial to acknowledge that this study focuses on spring dust sources of iron but pyrogenic iron sources, such as those from anthropogenic activities and biomass burning in other seasons also make a substantial contribution to the ocean's soluble iron inventory due to their high solubility (Ito et al., 2021; Ito et al., 2019; Rathod et al., 2020). The increased anthropogenic soluble iron deposition trend during our study period could opposite the decreased dust soluble iron deposition to some extent (Hamilton et al., 2020)."

Line 267: "The observations of iron used here is the total iron which include dust and pyrogenic iron. The simulated results are lower than observations likely due to the lack of pyrogenic iron. What's more, the comparison about iron solubility between simulation and observations has shown in Figure S7. Our model only captures the 0-10% iron solubility. This is likely due to the lack of pyrogenic iron which has been suggested to contribute to higher iron solubility (Ito et al., 2019)."

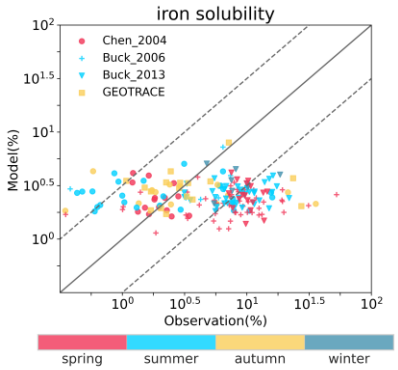

Figure S7. The comparison about iron solubility between simulation and observations.

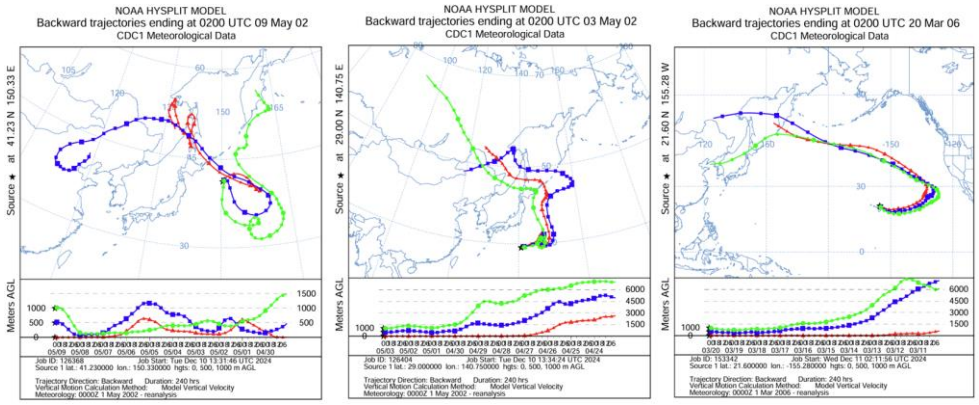

Figure. Examples of back-trajectory analyses

Reference

Buck, C. S., Landing, W. M., and Resing, J.: Pacific Ocean aerosols: Deposition and solubility of iron, aluminum, and other trace elements, Marine Chemistry, 157, 117-130, https://doi.org/10.1016/j.marchem.2013.09.005, 2013.

Chen, Y.: Sources and fate of atmospheric nutrients over the remote oceans and their role on controlling marine diazotrophic microorganisms, Doctoral dissertation, available at: https://drum.lib.umd.edu/handle/1903/1967, 2004.

Hamilton, D. S., Scanza, R. A., Rathod, S. D., Bond, T. C., Kok, J. F., Li, L., Matsui, H., and Mahowald, N. M.: Recent (1980 to 2015) Trends and Variability in Daily-to-Interannual Soluble Iron Deposition from Dust, Fire, and Anthropogenic Sources, Geophysical Research Letters, 47, e2020GL089688, https://doi.org/10.1029/2020GL089688, 2020.

Ito, A. and Miyakawa, T.: Aerosol Iron from Metal Production as a Secondary Source of Bioaccessible Iron, Environmental Science & Technology, 57, 4091-4100, 10.1021/acs.est.2c06472, 2023.

Ito, A., Myriokefalitakis, S., Kanakidou, M., Mahowald, N. M., Scanza, R. A., Hamilton, D. S., Baker, A. R., Jickells, T., Sarin, M., Bikkina, S., Gao, Y., Shelley, R. U., Buck, C. S., Landing, W. M., Bowie, A. R., Perron, M. M. G., Guieu, C., Meskhidze, N., Johnson, M. S., Feng, Y., Kok, J. F., Nenes, A., and Duce, R. A.: Pyrogenic iron: The missing link to high iron solubility in aerosols, Science Advances, 5, eaau7671, doi:10.1126/sciadv.aau7671, 2019.

Liu, M., Matsui, H., Hamilton, D. S., Rathod, S. D., Lamb, K. D., and Mahowald, N. M.: Representation of iron aerosol size distributions of anthropogenic emissions is critical in evaluating atmospheric soluble iron input to the ocean, Atmos. Chem. Phys., 24, 13115-13127, 10.5194/acp-24-13115-2024, 2024.

Rathod, S. D., Hamilton, D. S., Mahowald, N. M., Klimont, Z., Corbett, J. J., and Bond, T. C.: A Mineralogy-Based Anthropogenic Combustion-Iron Emission Inventory, Journal of Geophysical Research: Atmospheres, 125, e2019JD032114, https://doi.org/10.1029/2019JD032114, 2020.

Technical corrections

(1) Lines 121-123: Please rephrase. It is not obvious what the authors mean.

Response: Thank you for your insightful comment. We have added the global distribution of initial iron content in dust coarse mode aerosol as Figure S1(a) and expanded the discussion in line 137.

Line 138: "According to the utilization of the mineralogy map, our model achieved to simulate the global spatial patterns of total and initial soluble iron emissions. Compared to the default setting of 3.5%, the total iron content in dust aerosol is higher in the main dust sources including North Africa, Middle East and central Asia, and East Asia (Fig. S1a). This is consistent with the observations (Lafon et al., 2004, 2006; Shi et al., 2011b) and the research by Ito and Xu (2014), which reported that the observed iron content in North Africa and East Asia averaged 3.7%. Therefore, the use of the mineralogy map increases the iron content in dust from these regions (Fig. S1b) which suggest the default settings likely underestimate dust iron in these main dust source regions."

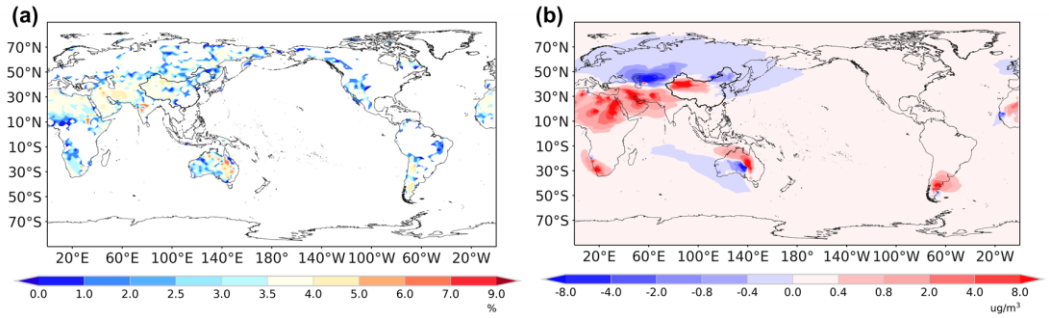

Figure S1. (a) Spatial distribution of iron content in coarse mode dust aerosol. (b) Compared to the default setting (3.5% iron in dust), changes in dust total iron surface concentrations from the developed model averaged 2001-2017 springs.

(2) Lines 252-254: Can you please also provide actual rates rather than just percentages? How are these numbers compared to other studies?

Response: Thank you for your insightful comment. Combined with the General comment#1, we have added the annually mean dust total/soluble iron deposition in the Northwest Pacific in Table 2 and compared with other studies in line 287.

Line 287:

"3.2 Spatial and temporal characteristics of dust iron deposition

3.2.1 Atmospheric dust iron budget

…For the Northwest Pacific, the simulated dust total and soluble iron burdens are 7.4 Gg and 0.11 Gg respectively. These values align with those reported by the Ensemble model. The simulated dust total and soluble iron deposition rates in the NWP are 589 Gg/yr and 10.1 Gg/yr which are consistent with results from both MIMI and the Ensemble model. But the NWP dust iron deposition reported by EC-Earth is higher than in our study due to differences in regional dust emissions."

(3) Section 3.2: Deposition rates could also be presented in a table.

Response: Thank you for your insightful comment. Combined with the General comment#1, we have added the annually mean dust total/soluble iron deposition in Table 2 in section 3.2.1.

Table 2. Global annual atmospheric dust total/soluble iron budget in 2017.

	Burden (Gg)		**Dry deposition (Tg/yr and Gg/yr)**		**Wet deposition (Tg/yr and Gg/yr)**		**Solu. Rate (Gg/yr)**	
	Fe_tot	Fe_sol	Fe_tot	Fe_sol	Fe_tot	Fe_sol	Fe_ps	Fe_os
Global	1331	15.4	42.7	445	66.5	874	129	200
coarse, fine	1301, 30	13.3, 2.1	42.2, 0.5	421, 24	65.4, 1.1	789, 85	78, 51	196, 4
NWP	7.4	0.11	0.05	1.2	0.54	8.9	1.3	1.73
coarse, fine	7.1, 0.3	0.09, 0.02	0.05, 0.001	1.1, 0.1	0.53, 0.01	7.8, 1.1	1.1, 0.2	1.68, 0.05

(4) Table 1: In general, all emissions come from CMIP6 with MEIC for China. Does this information really need to be repeated in the table? Moreover, why are chlorine emissions not presented in the table?

Response: Thank you for your insightful comment. We have removed the repeated words in the table. And the gas HCl is the model is not originated from primary emissions but secondary source.

(5) Figure 3: I propose to color-code only the seasons, not the 12 months of the year. It would probably make the figure less noisy.

Response: Thank you for your insightful comment. We have changed the color setting as follows.

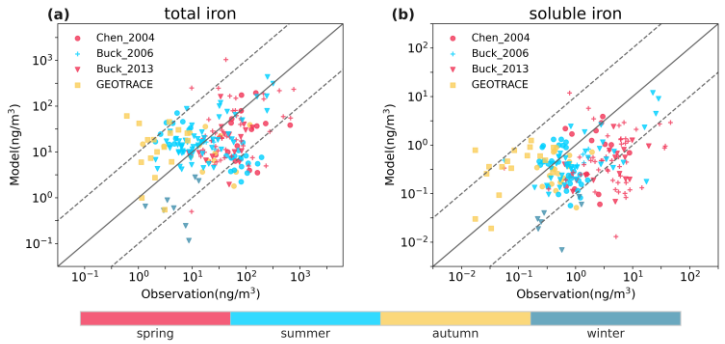

(6) In the whole manuscript: Better to change "oxalate-ligand-promoted" to either oxalate- or ligand-. Usually oxalate is used as a proxy for all organic ligands.

Response: Thank you for your insightful comment. We have replaced the "oxalate-ligand-promoted" to "oxalate-promoted".

(7) Line 343: The NCP abbreviation needs to be explained.

Response: Thank you for your insightful comment. We have explained the NCP in line 395.

Line 395: "… especially over North China Plain with intensive NO_x emission (Luo et al., 2020b)."

(8) Line 344: Please explain why HCl concentrations are increased in the model. How have precursor emissions changed?

Response: The gas HCl is the model is not originated from initial emissions but secondary source. In MOSAIC, the HCl gas are from irreversible heterogeneous reactions between acidic gases (such as HNO_3) and salt of chloride (NaCl and $CaCl_2$). It is the increased NO_x emissions induced higher HNO_3 gas and then more HCL are product. The increased HNO_3 gas has been shown in Figure S7. We have expanded the discussion in line 424 and corrected the earlier term of HCl emissions in line 458.

Line 424: "And the increasing trend in HCl concentration was induced by the enhanced HNO_3 gas which would produce HCl gases through heterogeneous reactions with NaCl/$CaCl_2$."

Line 458: "On the one hand, the increase in iron solubility can be attributed to enhanced NO_x/HCl concentrations and reduced dust emissions"

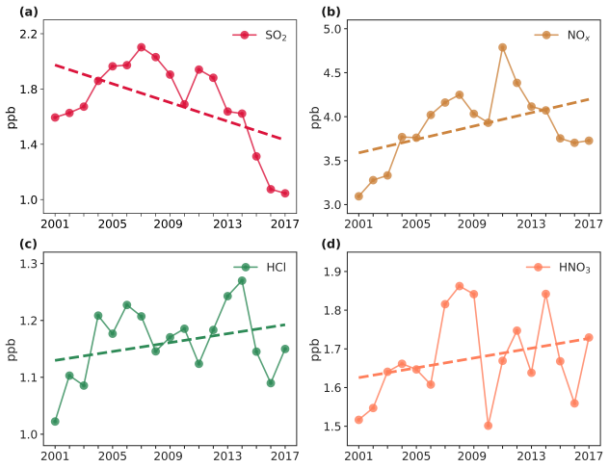

Figure S7. Temporal variations of surface concentrations of SO_2 (a), NOx (a), HCl (c), and HNO_3(d) over the high production rate of proton-promoted soluble iron area (30-45N, 120-150E) averaged of 2001-2017 springs.

(9) Lines 366-367: Can you please explain why aerosol water content is increased due to enhanced NO_x? How much has the coarse nitrate changed during the studied period? Please also discuss this, taking into account the general comments.

Response: Thanks for your insightful comment. We have corrected the mistake of 'coarse mode aerosol' to 'fine mode aerosol' in line 447. The decrease fine mode aerosol acidity over the mainland of EA could be attributed to the increased aerosol water content. This is caused by enhanced NO_x. Due to the high hygroscopicity of nitrate aerosol, the increased NO_x emissions would induce higher nitrate aerosol content and aerosol water content.

Specifically, aerosol water content in MOSAIC is calculated used Zdanovskii-Stokes-Robinson

(ZSR) mixing rule as the functions shown below:

$$W = \sum_{E=1}^{N} \frac{n_E}{m_E^0(a_w)}$$

where W is the aerosol water content, n_E is the number of moles of any electrolyte E in the solution, $m_E^0(a_w)$ is the binary electrolyte molality of E at the solution water activity which assumed a_w=RH. The increased nitrate content of high hygroscopicity would results in higher water content. The changes of fine nitrate aerosol and water content due to the increase NO_x emission experiment has shown in Figure S14.

We have corrected the mistake in line 447 and added the figure S14 to illustrate.

Line 366: "The decreased fine mode aerosol acidity over the mainland of EA could be attributed to the increased aerosol water content induced by enhanced NO_x (Figure S14).

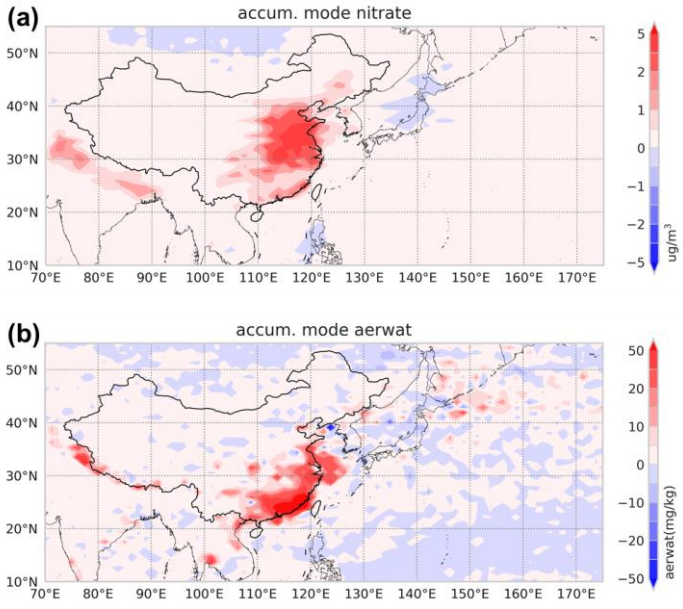

Figure S14. Spatial distributions of surface accumulation mode nitrate aerosol concentration (a) and aerosol water content (b) induced by NO_x experiment.